

Surface electronic structure of GaAs(001)-(2×4): Angle-resolved photoemission and tight-binding calculations

P. K. Larsen

Philips Research Laboratories, 5600 MD Eindhoven, The Netherlands

J. F. van der Veen

*FOM—Institute for Atomic and Molecular Physics, Kruislaan 407,
1098 SJ Amsterdam, The Netherlands*

A. Mazur and J. Pollmann

University of Dortmund, D-4600 Dortmund 50, West Germany

J. H. Neave and B. A. Joyce

Philips Research Laboratories, Redhill, Surrey RH1 5HA, England

(Received 8 February 1982)

We have carried out an experimental and theoretical study of the surface-energy-band structure of the As-stable GaAs(001)-(2×4) reconstruction. Angle-resolved photoemission measurements with the use of synchrotron radiation at LURE, Orsay, have been performed on surfaces which were grown *in situ* by molecular beam epitaxy. Measurements made at high-symmetry points and along symmetry lines of the surface Brillouin zone show weakly dispersing dangling-bond-like surface states in the energy range between -1.6 eV and the top of the valence band, and a nearly dispersionless state near -3 eV. To clarify the origin of these states, we have applied the scattering theoretical method on the basis of an empirical tight-binding description of the GaAs bulk crystal to the ideal (1×1) As-terminated surface and to a (2×1) asymmetric As-As dimer model. The principal effect of the reconstruction is the introduction of a new dimer-related state at -3.5 eV. In addition in the energy range near the top of the projected bulk bands, dangling-bond states with a significant in-plane component are found. Although we do not observe a direct one-to-one correspondence between experiment and theory, the essential features of an asymmetric As-As dimer are established.

I. INTRODUCTION

The determination of the electronic and crystallographic structures of clean, reconstructed GaAs{001} surfaces is of both fundamental and practical importance. Almost all device fabrication is based on this orientation, and with the advent of molecular beam epitaxy (MBE) (see, e.g., Ref. 1) as a viable thin-film-growth technique, it has become clear that film properties are closely related to surface conditions. At a more fundamental level it is probably the simplest polar surface of sphalerite lattice compounds to exhibit multiple reconstructions related to surface stoichiometry.

Previous studies of GaAs{001} surfaces have mostly been based on preparation by MBE and have included determination of the kinetics of sur-

face reactions,² evaluation of the relationships between surface stoichiometry and reconstruction,³⁻⁶ work-function measurements,⁵ electron-energy-loss spectroscopy,^{7,8} and angle-integrated and angle-resolved photoemission measurements.^{6,9,10} Theoretical treatments¹¹⁻¹³ have been confined to calculation of the surface energy-band structure for ideal, unreconstructed (1×1) Ga- and As-terminated surfaces. In recent angle-resolved photoemission results obtained from GaAs(001)-(2×4) surfaces prepared *in situ* by MBE,¹⁴ a prominent surface state has been identified at an initial-state energy (E_i) ~ 1 eV below the valence-band maximum (E_{VBM}). The intensity variation of photoemission from this surface state as a function of the polar angle θ suggested a surface model based on tilted (aplanar) dimers formed between

neighboring surface As atoms. This model is qualitatively similar to that proposed for the Si(001) surface¹⁵ and explains the doubling of the periodicity in the $[\bar{1}10]$ direction.

In the work reported here we have combined MBE with synchrotron-radiation-excited angle-resolved photoemission and reflection-electron diffraction (RED) to measure the surface energy bands for the GaAs(001)-(2×4) surface, which is the most stable reconstruction for this orientation. We find strong emission from surface states and surface resonances at initial energies between -3 eV and E_{VBM} . The emission is highly directional and particularly strong for off-normal emission, while the energy dispersions of the surface energy bands are rather weak.

In addition to the experimental investigation we have also calculated the surface energy-band structure by applying the scattering-theoretical method¹² to the ideal As-terminated surface and to a dimer model assuming a (2×1) surface structure. With the use of an empirical tight-binding bulk Hamiltonian, surface states and resonances were derived from a layer, orbital, and wave-vector-resolved density of states. By comparing experimental and theoretical surface energy-band positions we show that an As-dimerization model is in qualitative agreement with the experimental data.

The rest of the paper is organized in the following way: Section II contains a description of the experimental arrangement and Sec. III provides an outline of the method used for identification of surface states and illustrates its implementation. In Sec. IV further experimental results and their analysis in terms of surface energy bands are presented and discussed. Section V deals with the scattering theoretical method, emphasizing results of the calculations, and finally in Sec. VI the experimental results are compared with the calculations.

II. EXPERIMENTAL

Angle-resolved photoemission measurements were carried out using a system we have described previously,¹⁴ attached to the toroidal-grating monochromator (TGM) of the A61 beam line at the ACO storage ring (LURE, Orsay). The system is equipped with an hemispherical electron-energy analyzer, rotatable in the same horizontal plane as the incident radiation is polarized, four Knudsen sources for *in situ* MBE growth of GaAs and deposition of metal overlays, and a 5-keV RED fa-

cility for surface characterization.

Surfaces to be studied were prepared by growth on the GaAs(001) substrate surface, with the use of conditions to produce a (2×4) reconstruction (i.e., substrate temperature 790–820 K, As₄ to Ga flux ratio 3–6:1). The system pressure during growth rose to $\sim 1 \times 10^{-8}$ Torr, mainly due to As₄. After growth the substrate was cooled to room temperature, maintaining the (2×4) reconstruction, and photoemission measurements were made with typical angular and energy resolutions of 1.8° (full cone) and 0.2 eV (monochromator plus analyzer), respectively.

The grazing incidence TGM, which has a 161° total-deviation angle and two interchangeable gratings with 450 and 1200 lines mm⁻¹, is described in detail elsewhere¹⁶ and covers the photon-energy range 20–200 eV. The monochromatized radiation is $\sim 70\%$ polarized,¹⁷ and in general the polarization vector was chosen to make an angle of either 45° or 55° with the surface plane (mixed *s/p* polarization).

For the photon-energy range below 40 eV, which was used for much of the data presented here, spectra in the valence-band-energy region were superimposed on a smooth background produced by inelastically scattered electrons excited by second- and higher-order diffracted radiation from the grating. Although with the TGM used the second-order contribution is at most 7% of the first order, the energy dependence of the photon flux delivered by the ACO storage ring raises this to $\sim 30\%$ when the ring is being operated at 540 MeV. The background in the spectra can be significantly reduced by operating the ring at a lower energy; typically, a reduction in energy from 540 to 350 MeV reduces the background in spectra measured at the photon energy $h\nu=29$ eV by a factor of 2.

Higher-order radiation above 73 eV has been filtered out by transmission through 1500-Å-thick Al foils, in which absorption of radiation above the $2p_{1/2}$ and $2p_{3/2}$ absorption edges (73.1 and 72.7 eV, respectively) gave photoemission spectra background free at monochromator settings ≥ 37 eV. Similarly, Sn filters can be used for photon energies (first order) from 17.5 to 23.5 eV. In most cases, however, the smooth background was subtracted by taking pure background spectra at the photon energy corresponding to second-order radiation ($2h\nu$), using the same energy analyzer setting, and fitting this background to the energy region above E_{VBM} . We have checked the validity of this procedure wherever possible by comparison

with background-free spectra obtained either with HeI radiation or with one of the filters.

For all spectra shown in the following sections the initial-state binding energies are referred to E_{VBM} , which has been determined from the Ga $3d_{5/2}$ core-level position at the known bulk binding energy of 18.60 eV for GaAs.¹⁸

III. EXPERIMENTAL METHOD

A. The surface Brillouin zone

The primary purpose of our experimental study is to determine the surface energy-band dispersions $E_s(\vec{k}_{\parallel})$ (where \vec{k}_{\parallel} is the surface parallel wave vector), and in addition, to evaluate the bond orbital character at high-symmetry points in the two-dimensional surface Brillouin zone (SBZ). E_s should display the translational symmetry of the surface and have the periodicity of the SBZ,

$$E_s(\vec{k}_{\parallel} + \vec{g}_{\parallel}) = E_s(\vec{k}_{\parallel}),$$

where \vec{g}_{\parallel} is a surface reciprocal-lattice vector. The reduced parallel wave vector, being a conserved quantity in the photoemission process, should in principle be defined with respect to a SBZ having dimensions corresponding to the reconstruction. However, as we briefly mentioned in the introductory section and discussed at length previously,¹⁴ $[\bar{1}10]$ is the main ordering direction, i.e., the twofold periodicity along $[\bar{1}10]$ and *not* the fourfold periodicity along $[110]$ reflects the primary reconstruction. We shall show later that we indeed observe a twofold periodicity in the surface-band dispersion along $[\bar{1}10]$, whereas no fourfold periodicity is observed directly. In Fig. 1 we illustrate the (1×1) , (2×1) , and (2×4) SBZ's, using the symmetry point notation of Appelbaum *et al.*¹¹ but with a subscript added to indicate to which SBZ the symmetry point belongs. The GaAs lattice

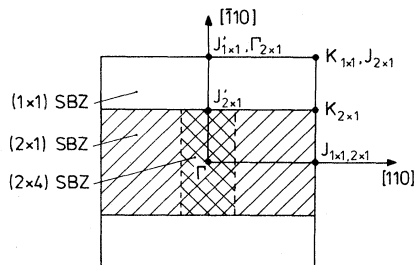


FIG. 1. Surface Brillouin zones for the (1×1) , (2×1) , and (2×4) reconstructions.

constant is $a = 5.654 \text{ \AA}$, so for the (1×1) SBZ $\Gamma K_{(1 \times 1)} = 2\pi/a = 1.111 \text{ \AA}^{-1}$ and $\Gamma J_{(1 \times 1)} = 0.786 \text{ \AA}^{-1}$.

We note that the number of surface energy bands is increased for a reconstructed surface with respect to the ideal surface and a simple backfolding of the (1×1) SBZ into a (2×4) SBZ would yield 8 times more bands from surface states and resonances with varying emission intensity in different SBZ's in the extended zone scheme. The strength of surface umklapp scattering determines whether a particular surface state can be observed in a given zone, thus all of these bands may not simultaneously be observed in any given zone. The finite angular resolution also plays an important role in this connection, since it leads to an uncertainty in the parallel wave vector \vec{k}_{\parallel} . This quantity is related to the electron kinetic energy E_k and the polar emission angle θ by the expression:

$$k_{\parallel} = \left[\frac{2m}{\hbar^2} E_k \right]^{1/2} \sin \theta, \quad (1)$$

from which it follows that

$$\Delta k_{\parallel} = \left[\frac{2m}{\hbar^2} E_k \right]^{1/2} \left[\frac{\sin \theta}{2E_k} \Delta E_k + \cos \theta \Delta \theta \right]. \quad (2)$$

For a typical kinetic energy of 25 eV and with our experimental resolutions of $\Delta E = 0.2 \text{ eV}$ and $\Delta \theta = 1.8^\circ$, one finds at near-normal emission that $\Delta k_{\parallel} \sim 0.08 \text{ \AA}^{-1}$, which amounts to about $\pm 20\%$ of the $\Gamma J_{(2 \times 4)}$ BZ-boundary momentum ($\Gamma J_{(2 \times 4)} = 0.196 \text{ \AA}^{-1}$). The finite resolution therefore makes it quite difficult to resolve the bands along the fourfold ordering direction, requiring a fourfold periodicity. This provides an argument for analyzing the data in terms of a (2×1) SBZ instead of a (2×4) . It is, of course, always possible from a plot of the surface energy bands in a larger SBZ to display them in a smaller one by backfolding the bands.

B. Identification of surface and bulk states

Observed spectral features in photoemission measurements may be due to surface states (we shall not always distinguish between surface states and surface resonances) or bulk states. To make a reliable assignment of the spectral features, we have used various approaches, which we discuss below.

One procedure often used to determine highly surface-sensitive features in the spectra is to quench the surface-state emission by adsorption of foreign atoms. The possibility of growing various surface structures by MBE provides us with a similar (and nondestructive) method, since surface states are characteristic of the surface structure. Figure 2 shows three spectra measured at the $K_{(1\times 1)}, J_{(2\times 1)}$ point under identical conditions, representing the clean surface (2×4) structure, the clean surface $C(4\times 4)$ structure, and a Pb-induced (1×3) structure. The latter was obtained with a Pb coverage of ~ 0.1 monolayers by deposition on a clean surface (2×4) structure at a substrate temperature below 570 K. For initial energies below ~ -2.7 eV the spectra are qualitatively very similar and this region corresponds predominantly to emission from bulk states. However, at energies higher than -2.7 eV the three spectra are quite different. The emission is strongly quenched by the Pb overlayer, while changing from a (2×4) to a $C(4\times 4)$ reconstruction significantly alters the energy positions of peaks and shoulders. On the basis of this, it might be concluded that the spectral features for $E_i \geq -2.7$ eV are dominated by surface-state emission and, notably for the (2×4) reconstruction, a very intense emission feature is observed at $E_i = -1.6$ eV. However, a change of the surface structure implies a change of surface reciprocal lattice vectors by which photoelectrons from bulk interband transitions can be elastically scattered (surface umklapp) and this mechanism can in principle also lead to different emission for different surface structures.¹⁹

A second criterion for the presence of surface states is that they should not disperse with the momentum perpendicular to the surface, \vec{k}_\perp , for a

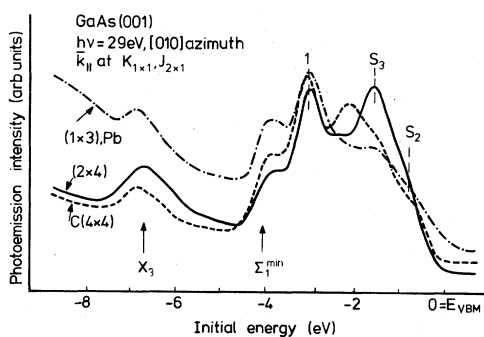


FIG. 2. Photoelectron-energy spectra taken at $\theta = 55^\circ$ and at a polar angle of 27° in the [010] azimuth for three different surface reconstructions. $\vec{k}_\parallel = \Gamma \bar{K}_{(1\times 1)}$ for $E_i = -1$ eV.

given \vec{k}_\parallel . By choosing an appropriate combination of photon energies and polar angles, \vec{k}_\perp can be varied while keeping \vec{k}_\parallel fixed at some point in the SBZ (this holds exactly only for one initial-state energy). Dispersion peaks can then be attributed to bulk interband transitions while stationary features are due to surface-state emission (apart from a few nondispersive bulk critical points). The application of this approach is illustrated in Fig. 3. The spectra were obtained at different photon energies and polar angles chosen to keep \vec{k}_\parallel equal to $\Gamma \bar{K}_{(1\times 1)}$ for $E_i = -1$ eV, which is the same choice of conditions as for Fig. 2. The two highly surface-sensitive features, S_2 and S_3 , observed in Fig. 2, are seen in Fig. 3 to be nondispersive, i.e., we have strong surface-state emission at $E_i = -1.6$ eV (S_3) and -0.9 eV (S_2) at the $K_{(1\times 1)}, J_{(2\times 1)}$ symmetry point.

The distinction between true surface states and surface resonances is that the former should lie in a gap of the projected bulk density of states. Figures 4(a) and 4(b) show projections for two different portions of the (1×1) SBZ. The point pattern is the projected bulk band structure. It is obtained by projecting all states of the bulk Brillouin zone (see Fig. 5) onto the (1×1) SBZ (shaded area in Fig. 5). Each point in the pattern corresponds to a bulk state $E_n(\vec{k}_\perp, \vec{k}_\parallel)$ for the given \vec{k}_\parallel , so that the density of points gives a visual impression of the density of projected bulk states for each \vec{k}_\parallel . Flat bulk bands (as a function of \vec{k}_\perp for a chosen \vec{k}_\parallel) give rise to a high projected density of states

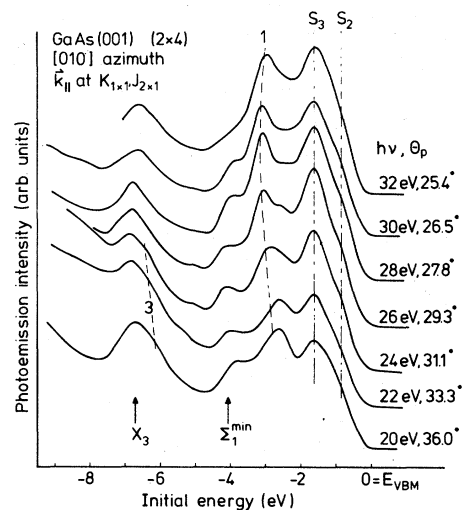


FIG. 3. Photoemission spectra taken at $\theta_i = 55^\circ$ in the [010] azimuth. The photon energies and polar angles are related to keep $\vec{k}_\parallel = \Gamma \bar{K}_{(1\times 1)}$ for $E_i = -1$ eV.

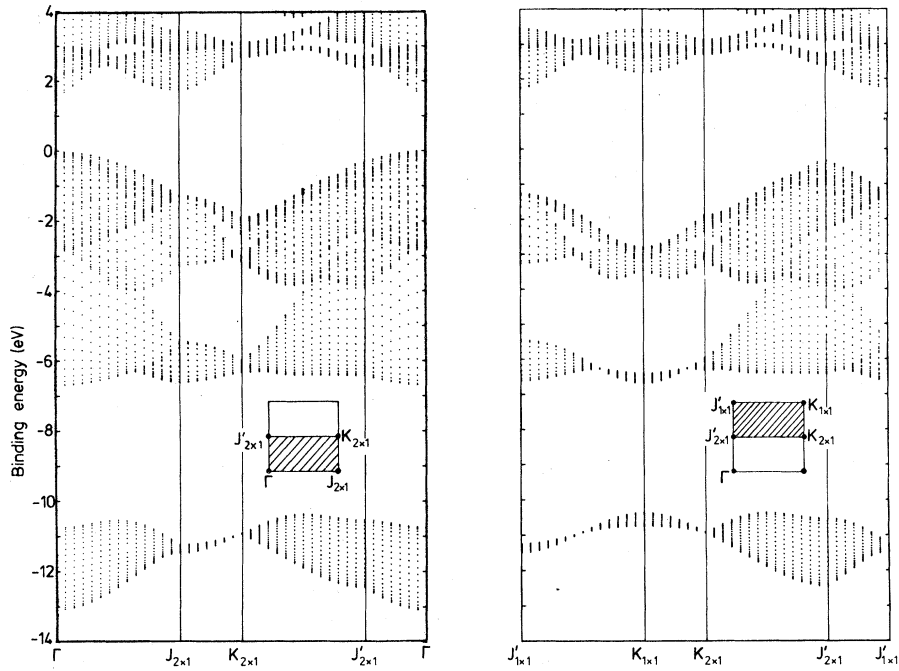


FIG. 4. Bulk band structure of GaAs projected on the (001) surface. The left- and right-hand panel show projections for the two different portions of the (1×1) SBZ shown as insets.

while strongly dispersive bulk bands yield regions of low projected density of states (and thus points). The two surface states mentioned above, S_2 and S_3 , have a value of \vec{k}_{\parallel} corresponding to the $K_{(1 \times 1)}$ symmetry point and from Fig. 4(b) we see that both states are situated in a band gap of the projected bulk band structure for the (1×1) SBZ. Surface state S_3 at the $K_{(1 \times 1)}$ point can couple to bulk states at the same energy by surface umklapp, which folds bulk states projected on the $J_{(2 \times 1)}$

point of the first (2×1) SBZ [Fig. 4(a)] onto the $K_{(1 \times 1)}$ point. S_3 is therefore not a true surface state but a surface resonance. However, the large intensity of S_3 suggests that its coupling to bulk states is weak. On the other hand, the complete absence of this state at the $J_{(2 \times 1)}$ point of the first (2×1) SBZ in the extended zone scheme may be explained by direct coupling to bulk states at the same energy [Fig. 4(a)]. The S_2 state remains in a bulk band gap of the (2×1) SBZ, but it may couple to bulk states through reciprocal lattice vectors of the (2×4) reconstruction.

A number of the spectral features observed can be directly assigned to transitions involving bulk states. It was shown recently by Chiang *et al.*²⁰ that for GaAs(110) the emission from valence-band states is well described by a direct-transition model and a quasi-free-electron final state assuming primary cone emission in the photon-energy range $25 \text{ eV} \leq h\nu \leq 100 \text{ eV}$. In previous work on MBE-grown GaAs(001)- (2×4) (Ref. 21), we showed that the same model explained very well the observed energy dispersion of the main bulk peaks down to final energies as low as 16 eV above E_{VBM} . In Fig. 3 the two broken lines marked 1 and 3 represent the calculated dispersion of direct transitions from

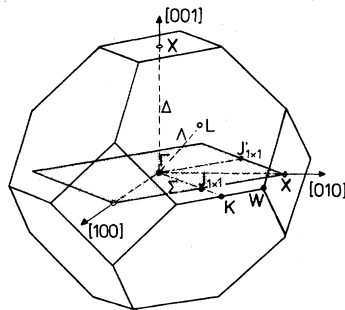


FIG. 5. Bulk Brillouin zone of GaAs with the (001)- (1×1) SBZ shown as an insert.

the valence bands to a quasi-free-electron final state (primary cone emission), and the agreement with the experimental dispersions is seen to be good. The less intense and weakly dispersing peaks which are often observed near the bulk critical point energies are attributed to direct transitions involving secondary cone and/or surface umklapp processes.²¹

The fact that the model just discussed applies so well makes it possible to avoid overlap of bulk interband transitions and surface-state transitions. As pointed out in Ref. 21 this is possible by choosing photon energies and polar angles such that the dispersing bulk move away from the surface features. Obviously, a necessary condition for this "tuning" of bulk transitions is that the bulk valence bands disperse with the surface perpendicular wave number k_{\perp} .

IV. EXPERIMENTAL DETERMINATION OF ENERGY VERSUS MOMENTUM DISPERSIONS

We present in this section our measurements of the energy dispersions of the surface energy levels. We have obtained angle-resolved photoemission spectra with \vec{k}_{\parallel} lying on the symmetry lines $\Gamma J'_{(2\times 1)}$, $\Gamma J_{(2\times 1)}$, $J'_{(2\times 1)}K_{(2\times 1)}$, and $J_{(2\times 1)}K_{(2\times 1)}$. The spectra shown in Fig. 6 were measured at $h\nu=29$ eV for a number of polar angles along the $[\bar{1}10]$ azimuth. There is a very prominent surface state, designated S_2 , whose initial energy has a dispersion of 0.3 eV, with a minimum value of $E_i = -1$ eV at normal emission (Γ point) and at $\theta = \pm 18^\circ$ ($J'_{(1\times 1)}$, $\Gamma_{(2\times 1)}$ points) and a maximum value of $E_i = -0.7$ eV for $\theta = \pm 9^\circ$ ($J'_{(2\times 1)}$ point). An energy dispersion versus \vec{k}_{\parallel} plot for this state shows that $E_i(\vec{k}_{\parallel})$ displays the twofold periodicity of the (2×1) SBZ along the $[\bar{1}10]$ azimuth. At and near normal emission, another surface state, labeled S_1 , appears as a weak shoulder on S_2 .

There are in Fig. 6 several peaks and shoulders at energies lower than $E_i = -1$ eV which can be ascribed to bulk features. The peaks labeled 1, 2, and 3 are due to primary cone emission from the upper three valence bands to a quasi-free-electron final state. They agree with calculated dispersions to within 0.2 eV typically. Band 1', which is also observed for the $C(4\times 4)$ reconstruction, and weak emission features near the energies of bulk critical points ($X_3, \Sigma_1^{\min}, X_5$) are attributed to direct bulk interband transitions involving secondary cone

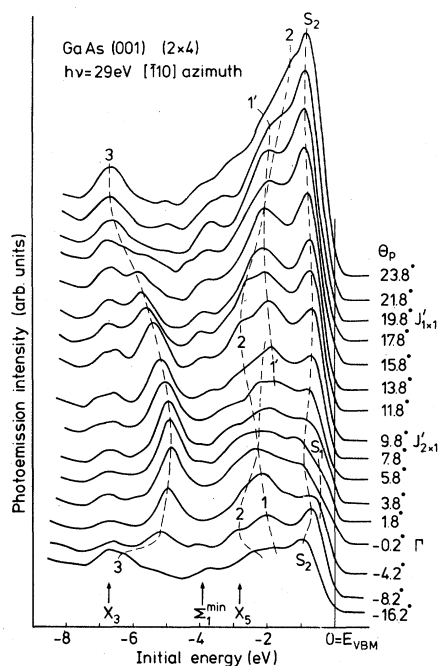


FIG. 6. Polar-angle dependence of photoemission for the (2×4) reconstruction taken at $\theta_i=45^\circ$ and $h\nu=29$ eV in the $[\bar{1}10]$ azimuth.

emission and/or surface umklapp processes.

At Γ the nature of the valence band giving rise to the bulk-related transition 3 is purely sp_z -like, and by comparing the angle-of-incidence (θ_i)

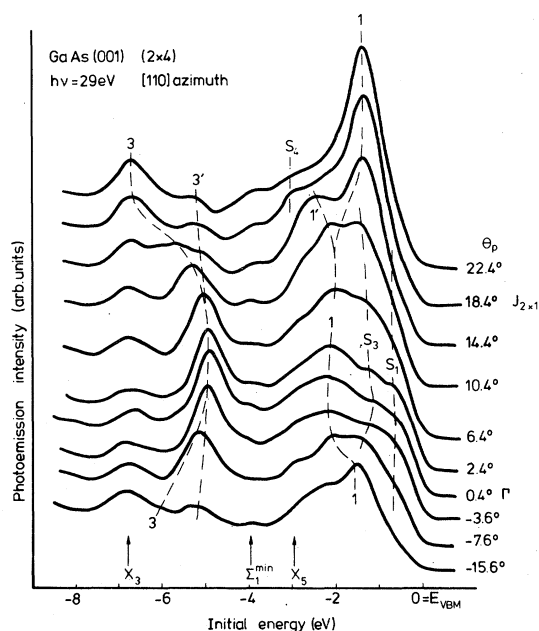


FIG. 7. Polar-angle dependence of photoemission for the (2×4) reconstruction taken at $\theta_i=45^\circ$ and $h\nu=29$ eV in the $[110]$ azimuth.

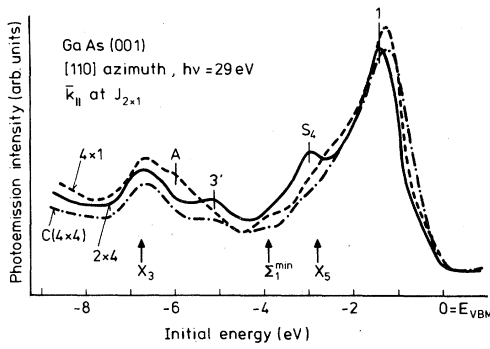


FIG. 8. Photoelectron-energy spectra taken at $\theta_i=45^\circ$, $h\nu=29$ eV, and at a polar angle of 18.8° in the $[110]$ azimuth for three different reconstructions.

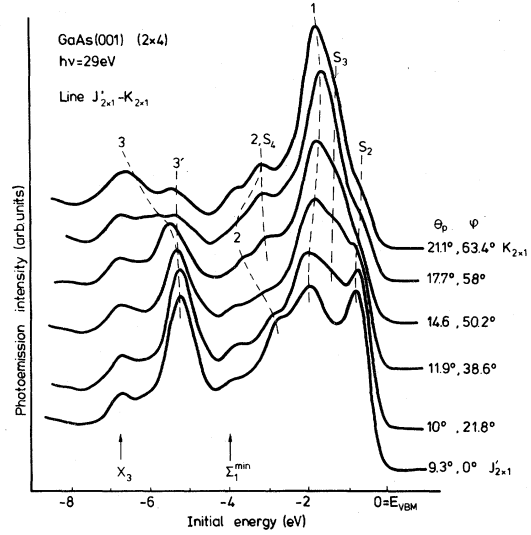


FIG. 9. Photoelectron-energy spectra taken at $\theta_i=45^\circ$ and $h\nu=29$ eV. The polar and azimuthal angles are related to keep $\vec{k}_{||}$ on the $J'_{(2\times 1)}K_{(2\times 1)}$ symmetry line for $E_i=-1$ eV.

dependence of the normal-emission intensity for this transition 3 with the surface states S_1 and S_2 , we find them both to be mainly sp_z -like. Each has some p_x character ($\hat{x}=[\bar{1}10]$), however, S_2 more than S_1 . This means, therefore, that both surface states are mainly dangling-bond related.

If we now consider the orthogonal azimuth (i.e., $[110]$), we observe quite different spectral behavior from that displayed in the $[\bar{1}10]$ azimuth over the energy region from the VBM to a few eV below.

Figure 7 shows spectra taken at $h\nu=29$ eV for several polar angles. The most significant difference is that the surface state S_2 , which was very pronounced along $[\bar{1}10]$, is no longer seen. Two

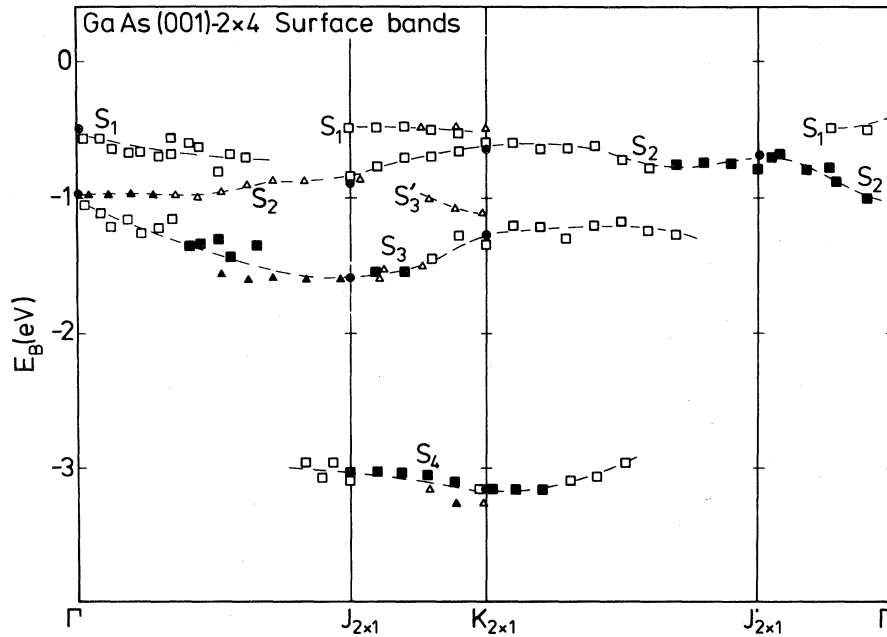


FIG. 10. Experimental surface energy bands for GaAs(001)-(2 \times 4) along the symmetry lines of the (2 \times 1) SBZ. \blacksquare , \square : Peaks, (shoulders) measured at $h\nu=29$ eV. \blacktriangle , \triangle : Peaks, (shoulders) measured at $h\nu=21.2$ eV (from Ref. 14). \bullet : Measured at various photon energies in the range 20–32 eV.

other surface states, S_1 and S_3 , are present in this energy region, but their dispersion cannot easily be followed because of the dispersion and dominance of the bulk feature 1, especially at the larger polar angles. In addition to this feature 1, those marked 1', 3, and 3' can all be identified with bulk interband transitions, and there are also peaks and shoulders at energies corresponding to the critical points.

A peak marked S_4 is observed at $E_i \sim -3$ eV for polar angles corresponding to \vec{k}_{\parallel} close to the symmetry point $J_{(2 \times 1)}$, but it shows no k_{\perp} dispersion ($h\nu$ dependence) at $\vec{k}_{\parallel} = \bar{\Gamma} J_{(2 \times 1)}$ for $E_i = -3$ eV. Although this fulfills a necessary condition for this state to be surface related, it is close in energy to the X_5 critical point at -2.8 eV,²⁰ which may confuse the spectra. We have therefore checked its origin by comparing spectra for three different GaAs(001) surface reconstructions, and as shown in Fig. 8, S_4 is reconstruction dependent. We conclude that it is not related to a bulk critical-point transition, but is in fact a surface state.

Finally, we will comment briefly on spectra obtained with \vec{k}_{\parallel} following the symmetry lines $J'_{(2 \times 1)} K_{(2 \times 1)}$, shown in Fig. 9. The polar and azimuth angles have been chosen to keep \vec{k}_{\parallel} on this symmetry line for $E_i = -1$ eV, and \vec{k}_{\parallel} does not fall on the line at other initial energies. However, the difference is rather small in a range of a few eV around $E_i = -1$ eV (e.g., at the $K_{(2 \times 1)}$ point and $E_i = -4$ eV, $\vec{k}_{\parallel} = 0.93 \bar{\Gamma} K_{(2 \times 1)}$). The surface state S_2 at $E_i = -0.7$ eV has maximum intensity near the $J'_{(2 \times 1)}$ point and is only seen as a shoulder at the $K_{(2 \times 1)}$ point, while the S_4 state is observed at $E_i \sim -3.15$ eV, overlapping the bulk interband transition 2, near the $K_{(2 \times 1)}$ symmetry point.

On the basis of these measurements and those reported earlier¹⁴ using unpolarized He I radiation, we are now in a position to map out the experimental surface energy-band structure for GaAs(001)-(2×4), as shown in Fig. 10 in the frame of the (2×1) SBZ. In the next section we present our calculated version of this band structure, and in the final section we compare experiment with calculation.

V. THEORY

In this section we present the results of our theoretical investigation of the ideal and the reconstructed GaAs(001) surfaces. We have employed

the scattering theoretical method^{12,22} on the basis of an empirical tight-binding description of the GaAs bulk crystal. This method allows truly semi-infinite solids to be treated. A detailed account of the formalism as it applies to relaxed or reconstructed surfaces will be given elsewhere.²³ Here we only briefly summarize the basic equations.

A. Basic equations

The formal treatment can be cast into three distinct steps. We start with an unperturbed, three-dimensional periodic bulk crystal, described by the Hamiltonian H^0 . In the present study we used a carefully determined empirical tight-binding Hamiltonian. The surface is then introduced by removing sufficient layers to produce two noninteracting, semi-infinite crystals. Furthermore, the lattice-geometry changes near the surface need to be included. All this can be accomplished by a perturbation matrix U which is highly localized perpendicular to the surface (for details, see Refs. 22, 23, and 12). In the final step, the changes induced by the perturbation U in the one-particle spectrum of H^0 are calculated exactly by solving the eigenvalue problem of the full Hamiltonian H ,

$$H\psi = (H^0 + U)\psi = E\psi, \quad (3)$$

which describes a semi-infinite solid with a properly reconstructed surface. All model assumptions about the type of reconstruction enter the perturbation matrix U . The formal solution of Eq. (3) is given by the Lippman-Schwinger equation

$$\psi = \varphi + G^0 U \psi, \quad (4)$$

where φ represents the homogeneous solution (i.e., in our case the bulk Bloch functions) and ψ are the eigenstates of the semi-infinite solid. The Green's function of the unperturbed system, i.e., the bulk Green's function $G^0(E)$ is defined as

$$G^0(E) = \lim_{\epsilon \rightarrow 0^+} (E + i\epsilon - H^0)^{-1}. \quad (5)$$

In energy regions where no solutions for the bulk crystals exist (i.e., in the projected gaps and pockets) and φ vanishes, new bound states may occur according to Eq. (4) if

$$\det |1 - G^0(E)U| = 0 \quad (6)$$

has nontrivial solutions. According to the short-range nature of U , the size of the matrices that need to be calculated in Eq. (6) is very small.

Resonances in the bulk band continua can be studied by calculating the density of states

$$N(E) = -\frac{1}{\pi} \text{Im Tr} G(E), \quad (7)$$

where $G(E)$ is the Green's function of the semi-infinite crystal. It can be evaluated by solving Dyson's equation

$$G(E) = G^0(E) + G^0(E)UG(E). \quad (8)$$

Owing to the short-range character of U , Eq. (8) can be solved. Representing the operators in a layer-orbital basis leads to layer-, orbital-, and wave-vector-resolved densities of states given by

$$N_{m,\alpha}(\vec{k}_{\parallel}, E) = -\frac{1}{\pi} \text{Im} \langle m, \alpha, \vec{k}_{\parallel} | G(E) | m, \alpha, \vec{k}_{\parallel} \rangle. \quad (9)$$

Here m labels the layers, α labels the orbitals in the two-dimensional unit cell, and \vec{k}_{\parallel} is the wave vector running through the first SBZ. Equation (9) allows a detailed analysis of surface-induced features to be made, since it determines the localization (m), the orbital character, and thus the symmetry (α) for any given structure in the local density of states (LDOS) at a particular energy E with wave vector \vec{k}_{\parallel} .

For the bulk description we have used our empirical tight-binding Hamiltonian, which contains first- and second-nearest-neighbor interactions. The parameters are listed in Table I. This Hamiltonian provides a very good description of the valence bands and also reproduces measured energies of the lower conduction bands of GaAs at high-symmetry points very accurately. It was obtained by fitting both the bulk valence-band data of Chiang *et al.*²⁰ and the reflectivity data of Aspnes *et al.*²⁴

B. The ideal As-terminated surface

We first present the electronic structure of the ideal (1×1) surface to establish a well-defined basis for the discussion of reconstruction-related effects which we treat subsequently. In Fig. 11 we show the surface band structure for the ideal (1×1) surface. Solid lines represent bound surface states and dashed lines indicate the peak positions of pronounced resonances. The point pattern shows the nature and origin of the various surface states it is most helpful to consider the creation of the (001) surface, which leaves two broken sp^3 -hybrid bonds per surface unit cell (see the schematic Fig. 12). Since these two broken bonds are localized at the same atom, they interact very strongly giving rise to a pronounced dehybridization, and consequently their symmetry character is entirely changed. The two resulting bonds are very different (see Fig. 12). One is the sp_z -mixed dangling bond, which is oriented perpendicular to the surface, and the other is the p_x - p_y mixed bridge bond, oriented along the $[\bar{1}10]$ direction. These surface bonds give rise to the dangling-bond and bridge-bond bands D and B , respectively. Since the dangling bond contains strong s contributions it lies lower in energy than the bridge bond. The latter extends as a true bound state throughout the SBZ. The dangling-bond band becomes resonant with bulk states between Γ and $J'_{(1 \times 1)}$ as well as Γ and $J'_{(1 \times 1)}$. The changes in bonding configuration near the surface, in addition, give rise to a p -like back-bond state B and to predominantly s -like back-bond states. One of them (S_c) is mainly cation derived while the other (S_a) is mostly anion derived. The pronounced resonance within the projected As bulk bands around -12 eV is, of course, As derived. This resonant feature is mainly localized on the third layer. The ideal As-terminated polar surface is metallic, as shown by electron counting. There are two broken bonds per surface unit cell, each containing $\frac{5}{4}$ electrons. Putting these 2.5 electrons per unit cell into the dangling-bond and bridge-bond bands leaves the dangling-bond band fully occupied while the bridge-bond band is only partially

TABLE I. Tight-binding parameters in eV for GaAs (standard notation; see, e.g., Ref. 30).

	E_s	E_p	V_{ss}^2	$V_{pp\sigma}^2$	$V_{pp\pi}^2$	V_{ss}	V_{sp}^{CA}	V_{sp}^{AC}	$V_{pp\sigma}^1$	$V_{pp\pi}^1$
Anion	-7.51	0.28	-0.03	0.40	0.049	-1.762	1.983	2.455	2.487	-0.318
Cation	-3.0	1.402	-0.05	0.645	-0.163					

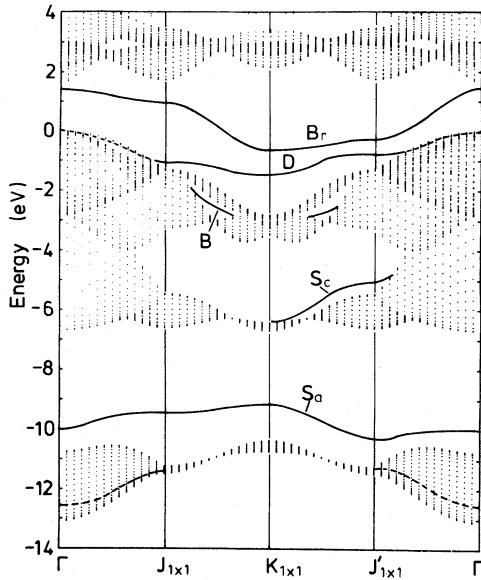


FIG. 11. Surface band structure and projected bulk bands for the ideal As-terminated GaAs(001)-(1×1) surface. The bands labeled B_r , D , and B are derived from the bridge bond, the dangling bond, and the back bonds, respectively. S_c and S_a represent cation- and anion-derived s -like back-bond states.

filled with 0.5 electrons. This result is in contradiction to the experimental findings for the real, i.e., the reconstructed surface, which is semiconducting.

C. Computational procedure for the reconstructed surface

We have shown previously¹⁴ that the As-rich GaAs(001) surface undergoes a (2×4) reconstruction with the 2× reconstruction being the dominant ordering mechanism. We therefore concen-

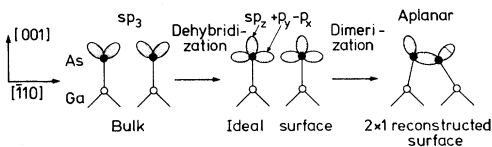


FIG. 12. Schematic diagram of the two disrupted sp_3 lobes per surface atom on a newly created (001) surface (left-hand part), the dehybridized dangling bond (sp_z) and bridge bond ($p_y - p_x$) on the ideal surface (middle part), and the asymmetric dimer model for the reconstructed (2×1) surface (right-hand part). The hatching indicates the number of electrons per bond.

trate on investigating the effects introduced by this strong 2× reconstruction. We expect that the ×4 reconstruction gives rise only to less-pronounced effects on the surface band structure. We will, therefore, discuss the (2×1) reconstructed surface in the following.

The surface Brillouin zone of the (2×1) surface is shown in Fig. 1 and the reconstruction-induced backfolding of bulk states has been discussed in Sec. III B (see also Fig. 4). Plotting the surface band structure of the ideal (1×1) surface along high-symmetry lines of the (2×1) surface Brillouin zone yields Fig. 13. The backfolding process superimposes the projected bulk states of Figs. 4(a) and 4(b) onto the (2×1) surface Brillouin zone and the ideal surface states also must be folded back. In Fig. 13 the surface-state bands between $K_{(2\times 1)}$ and $J'_{(2\times 1)}$ are all twofold degenerate (apart from spin degeneracy) since the $K_{(2\times 1)}J'_{(2\times 1)}$ line is folded onto itself. A comparison of Figs. 11 and 13 shows that the gaps and pockets free from projected bulk states have become smaller. In particular, some parts of the ideal surface-state bands have become resonant with bulk states in Fig. 13 due to the reconstruction-induced surface umklapp.

For a full description of the reconstruction we must now take into account the new atomic posi-

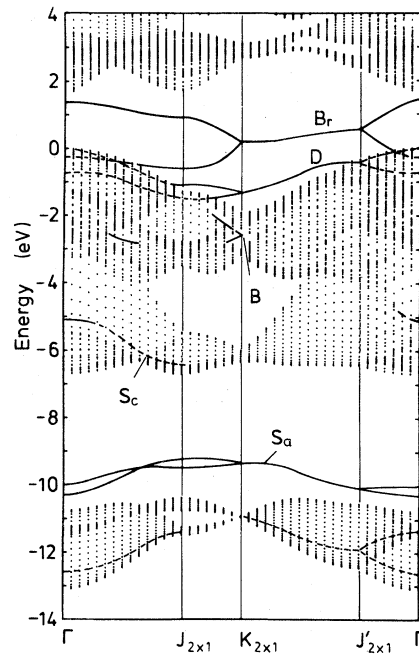


FIG. 13. Surface band structure and projected bulk bands for the ideal As-terminated GaAs(001) surface back folded onto the (2×1) SBZ. The bands are labeled as in Fig. 11.

tions at the reconstructed surface together with the corresponding changes in the interactions between the atoms. These reconstruction-induced changes of interactions, as compared to the ideal surface, may in general shift or split the backfolded ideal surface states. Certainly, the twofold degeneracy of the bands between $K_{(2 \times 1)}$ to $J'_{(2 \times 1)}$ in Fig. 13 will be lifted and even more importantly, the backfolded dangling bonds and bridge bonds may now strongly interact.

To carry out the calculations according to the formalism we need a reconstruction model and we have to specify the perturbation matrix U that formally incorporates the new surface geometry and the corresponding reconstruction-induced change in the interactions. We have used in our calculations an asymmetric dimer model very similar to that for the Si(100) surface proposed by Chadi on the basis of energy-minimalization calculations.²⁵ Most of the semiconductor surfaces tend to undergo reconstructions (or relaxations) that leave an asymmetric dimer per unit cell with the more electronegative ion moved outwards and the more electropositive ion moved inwards. Charge transfer from the down atom to the up atom reduces the electrons kinetic energy, its exchange correlation energy, and increases the attractive electron-ion interaction thus stabilizing the new geometry by minimizing the total energy. This general type of "charge-transfer relaxation" has been observed for Si(111)-(2 × 1), Si(100)-(2 × 1), GaAs(110), ZnO(10 $\bar{1}$ 0), and many other (similar) surfaces. We, therefore, think it to be a very meaningful start to study an asymmetric dimer model for the As-terminated 2 × 1 surface of GaAs(001). The dimerization of the two As-atoms per surface unit cell is schematically shown in Fig. 12. We start with the broken bulk sp^3 -hybrids which are dehybridized into a dangling and a bridge bond at the ideal surface. At the reconstructed (2 × 1) surface two As atoms which have been second-nearest neighbors at the ideal surface are moved inwards and closer together without changing the first-nearest-neighbor distance to the Ga atoms in the second layer. This inward movement is different for the two atoms so that an asymmetric dimer results. The new coordinates of the two atoms which were originally located at (0,0,0) and ($-a/2, a/2, 0$) are specified by (in units of Å):

$$\begin{aligned} \Delta x_1 &= 0.460, & \Delta z_1 &= -0.077, \\ \Delta x_2 &= 1.242, & \Delta z_2 &= -0.580, \end{aligned} \quad (10)$$

with Δx_i being measured along the $[\bar{1}10]$ direction.

Note, that the As-As distance in the dimer is nearly a first-nearest-neighbor distance of the GaAs lattice. This fact faces us with a new problem since there are no first-nearest-neighbor As-As interactions in bulk GaAs. Usually, in tight-binding calculations for reconstructed surfaces (see, e.g., Refs. 23, 25, and 26) one uses a d^{-2} scaling law for the interaction matrix elements, where d is the distance between the interacting orbitals. That law, however, can be used only for relatively small distance changes. Therefore, we cannot simply take As-As second-nearest-neighbor interactions from our accurate bulk Hamiltonian and scale them up to a first-nearest-neighbor distance. Instead we used the following procedure which gives a reasonable first estimate for the interaction matrix elements, as we will show. To obtain these interaction parameters, which are given in Table II, we first calculated the bulk band structure of GaAs with the use of a localized basis set with Gaussian orbitals and the empirical Ga and As pseudopotentials given in Ref. 27. From these results we could calculate the set of the tight-binding parameters necessary to reproduce this GaAs band structure. These parameters are, of course, not identical to those given in Table I which reproduce the experimentally determined energy bands of GaAs. In the next step we put the As pseudopotential on each lattice site of the GaAs lattice and calculated the corresponding band structure. This band structure was also reproduced by a tight-binding calculation and we are now able to determine the relative strength of the first-nearest-neighbor As-As interactions with respect to the first-nearest-neighbor Ga-As interactions. Finally, we multiply our tight-binding parameters (Table I) with the ratio of the As-As and Ga-As interaction parameters as determined by the pseudopotential calculations. The resulting parameters for the first-nearest-neighbors As-As interactions are listed in Table II.

D. Electronic structure of the (2 × 1) asymmetric dimer model

In this section we want to discuss our results for the (2 × 1) reconstructed surface. The surface band

TABLE II. Tight-binding parameters in eV for first-nearest-neighbor As atoms.

V_{ss}	V_{sp}	$V_{pp\sigma}$	$V_{pp\pi}$
-1.51	2.15	2.42	-0.31

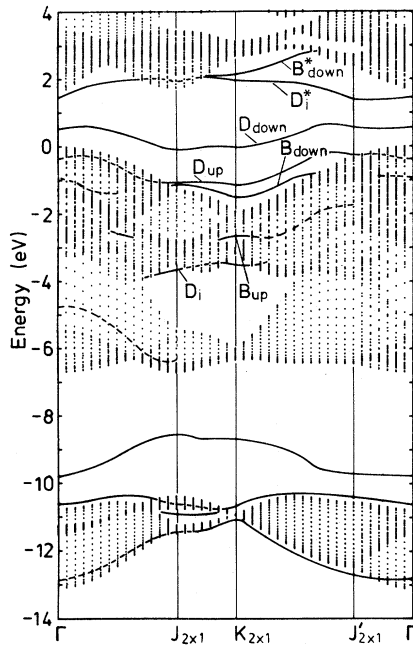


FIG. 14. Surface band structure and projected bulk bands for the (2×1) asymmetric dimer model with the As-As distance in the dimer equal to a first-nearest-neighbor distance in GaAs (for details, see text). The labeling “up” and “down” refers to the up and down atom of the dimer. The bands labeled D , D_i , and B represent states derived from the dangling bonds, the dimer bond, and the back bonds, respectively.

structure for the asymmetric dimer model is shown in Fig. 14. To understand the origins and the nature of the new states at the reconstructed surface it is very helpful to consider the reconstruction-induced changes from the ideal surface to the fully reconstructed surface in distinct steps. Before we discuss the surface-state bands in Fig. 14, we will, therefore, first investigate how the change in atomic positions influences the surface states at $K_{(2 \times 1)}$ in the energy range between -4 and $+3$ eV. The point $K_{(2 \times 1)}$ corresponds to the midpoint of the $J_{(1 \times 1)}K_{(1 \times 1)}$ line of the ideal surface Brillouin zone. We see in Figs. 11 and 13 that there are three bound surface states in this energy interval at the ideal surface. They are all twofold degenerate in Fig. 13. In Fig. 15 we show the changes in the layer densities of states per unit cell on the first four layers with respect to the corresponding bulk layer densities of states for five different As-As distances in the surface unit cell. The left-hand panel (a) shows the result for the ideal surface, while the right-hand panel (e) shows the result for

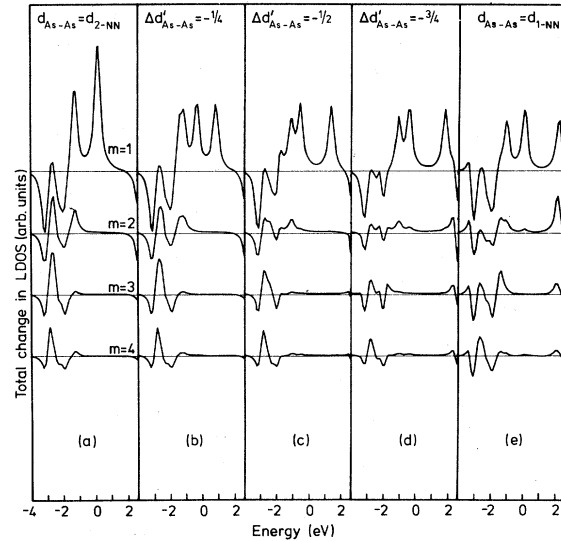


FIG. 15. Total changes in the layer densities of states per unit cell for the $K_{(2 \times 1)}$ symmetry point on the upper four layers ($m = 1, \dots, 4$) with respect to corresponding bulk layer densities of states. The five panels represent five As-As dimer distances, $d_{\text{As-As}}$. In the left and right panel $d_{\text{As-As}}$ equals the second- and first-nearest-neighbor distances ($d_{2\text{-NN}}$ and $d_{1\text{-NN}}$), respectively. In the three middle panels $d_{\text{As-As}} = d_{2\text{-NN}} + d'_{\text{As-As}} \times (d_{2\text{-NN}} - d_{1\text{-NN}})$ with $d'_{\text{As-As}} = -\frac{1}{4}, -\frac{1}{2},$ and $-\frac{3}{4}$.

the fully reconstructed asymmetric dimer according to our model. The three middle panels are obtained by changing the As-As distance from the ideal to the reconstructed one in $\frac{1}{4}$ steps. The LDOS changes clearly reveal for the ideal surface the three twofold degenerate bound states seen in Fig. 13. The state at 0.2 eV is the bridge bond consisting of 98% p character along the $[\bar{1}10]$ direction. The dangling-bond state is at -1.2 eV and is built up out of s states (12%) and p_z states (84%). The third state at -2.7 eV is back-bond related, since it is localized on the second, third, and fourth layers as is clearly demonstrated by Fig. 15(a). This feature changes its wave-function character from layer to layer, since the two sp^3 hybrids involved in connecting consecutive layers change their orientation by 90° on every other layer. If we now move the As surface atoms pairwise closer together [Figs. 15(b)–15(e)] the previously discussed states start to interact. Shifts and splittings of the features occur. In Fig. 15(b) we see that the bridge bonds are more strongly split than the dangling bonds, which is not surprising if one considers the schematic Fig. 12. If we bring the As atoms closer

together, the bridge-bond lobes immediately start to increase their overlap drastically while the dangling lobes are less perturbed. In addition, the interaction of the bridge bonds is a $pp\sigma$ interaction while the dangling bonds interact only via π -matrix elements. Note that the back bond at -2.7 eV is almost unaffected due to its back-bond nature.

If we now proceed to Fig. 15(c), the splitting of the two former bridge bonds becomes so large that the lower of the two coincides initially with the two slightly split dangling-bond-derived states and the three interact strongly with one another. Three distinct and well-separated peaks result near -0.5 , -1 , and -1.7 eV, belong to the three mixed states. The back-bond state near -2.7 eV decreases a little in amplitude on the second and third layer without changing its energy position significantly. Note, however, that for this separation of the As surface atoms a second new feature splitting off the back-bond state is introduced. This is easy to explain. In our asymmetric dimer model the distance of the two As-dimer atoms to the lower layers becomes increasingly different so that the back-bond peak splits. One of these distances remains almost constant while the other one shortens. A new structure is therefore split off the back-bond peak on the high-energy side while one of the former states stays fixed near -2.7 eV. The situation shown in the fourth panel is similar to case (c), where the splittings and shifts have further increased.

The final result for the full asymmetric dimer is given in the last panel where we have again labeled the various peaks in order to indicate their nature. Near 2.2 eV we find the split-off former-bridge-bond state which has now become an antibonding dimer state. Near 0 eV we find a dangling-bond state which is localized at the down atom (see Fig. 12). This state consists of 80% p_z character and 12% p character along $[\bar{1}10]$, proving its dangling-bond character and showing that the dangling-bond lobe is slightly tilted with respect to the surface normal. The state at -1.1 eV is another dangling-bond state localized at the up atom. On the first layer, its LDOS consists of 73% p_z contributions and 11% s contributions. This higher s character, as compared to the other dangling bond, is the reason for the lower energy of this state. Very near to this dangling bond we see a new back-bond state with relatively high density on the second and third layer. This state corresponds to the back bonds of the down atom and is now strongly split off from the other back bond

remaining near -2.7 eV [as discussed for Fig. 15(c)]. In addition, a new state near -3.5 eV is found at the reconstructed surface. This state originates from the newly established dimer-bond at the surface (see Fig. 12). The increase of the LDOS corresponding to this state is purely p like and is directed along the $[\bar{1}10]$ direction, i.e., the dimer direction.

We have summarized the previously discussed changes of the energy positions of the surface states as a function of the As-As distance in the dimer in Fig. 16. The shaded bands are regions of projected bulk states at $K_{(2\times 1)}$ (see also Fig. 13). We have tentatively connected the calculated points by dashed lines revealing the general reconstruction-induced interaction pattern of the various states. The figure shows how large the splittings and shifts of bound state levels can be, if we go from an ideal to the reconstructed surface. Uncertainties in the As-As interaction matrix elements of the surface dimer are, therefore, not expected to influence this picture significantly.

Having discussed the nature of the surface states for one particular \vec{k}_{\parallel} value in great detail, let us now summarize the main features of the full surface-band structure, as given in Fig. 14. The band D_i^* is the antibonding dimer band. The bands D_{down} and D_{up} are the two dangling-bond

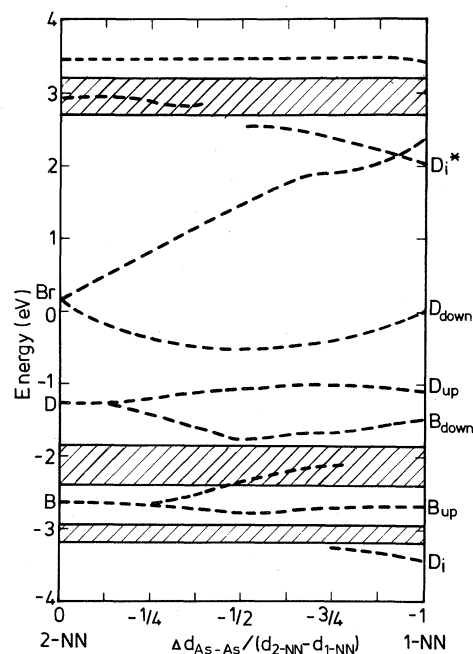


FIG. 16. Energy positions of surface bands for the $K_{(2\times 1)}$ symmetry point vs the As-As dimer distance.

bands discussed above. The down-atom dangling bond gives rise to band D_{down} , while the up-atom dangling bond yields band D_{up} . The band D_i is the new dimer-induced bonding band, i.e., the bonding counterpart to D_i^* . Furthermore, two entirely new reconstruction-induced bands B_{down} and B_{down}^* occur. They originate from the down-atom-induced back bonds and are bonding (B_{down}) and antibonding (B_{down}^*) in nature. The up-atom back-bond gives rise to the band near -2.7 eV at $K_{(2\times 1)}$ which extends as a very pronounced resonance to $J'_{(2\times 1)}$: In the energy range between -4.8 and -6 eV we find, in addition, a strong resonance. By comparing Figs. 13 and 14, it becomes obvious that this resonance is essentially the backfolded S_c band of the ideal surface. While the S_c band is only very slightly affected by the reconstruction, the anion-derived back-bond band S_a strongly splits due to reconstruction-induced interactions. This, of course, follows from the fact that the reconstruction introduces new As-As interactions and yields only very small indirect changes in the Ga-Ga interactions. The splitting of the backfolded S_a bands is essentially determined by the V_{ss} interaction of the neighboring As dimer atoms. One of the split bands is shifted further upwards within the heteropolar gap. The other is shifted downwards in energy and nearly coincides with the upper edge of the joint-projected bulk GaAs states, which are known to be mainly As derived. The additional s -like As resonance within these projected As bands is slightly shifted down in energy and splits between $J_{(2\times 1)}$ and $K_{(2\times 1)}$ into a resonance band and a bound-state band. Since it is mainly located on the third and fourth layer, it does not show any stronger effects.

VI. DISCUSSION

If we consider first the influence of a (2×1) reconstruction, produced by As-As dimerization, on the surface band structure, we can see by comparison of Figs. 13 and 14 that the major effect is in the energy region corresponding to the sp bonding bands, between -4 eV and the VBM. This is similar to our experimental findings. If we now compare theoretical predictions with experimental results for this energy region, the most striking agreement is that between the calculated dimer-bond-related state D_i and the observed state S_4 . From Fig. 16 it is clear that the calculated energy position of the state D_i is rather sensitive to the precise model used, e.g., it is only found below

-3 eV for the shortest As-As distances used. If one considers panel (e) of Fig. 15, the impression might be created that the dimer bond is only a weak feature in the LDOS. This occurs because in the figure it is the change in the density of states between the (2×1) reconstructed surface and the bulk LDOS which is plotted. If instead we consider the difference in the LDOS between the (2×1) reconstructed surface and the ideal (1×1) surface, however, a strong dimer-induced feature is observed. This means that the dimer formation is tending to reestablish a bulk-like sp bond. It therefore lies close to the projected bulk bands, and it is obvious that it does not occur on those reconstructed surfaces which do not result from As-As dimerization [cf. Fig. 8 for the $C(4\times 4)$ surface].

Closer to the top of the projected valence bands, dangling-bond states are found both experimentally and theoretically. The symmetry of the calculated dangling-bond states shows substantial p_y - p_x character, indicating the tilted nature of these bonds. Experimentally, we find at Γ for states S_1 and S_2 a similar in-plane characteristic. However, there is not, nor should be expected, a one-to-one correspondence between observed and calculated states. The most important difference is that the prominent surface state observed at -1.6 eV at the $J_{(2\times 1)}, K_{(1\times 1)}$ symmetry point does not appear in the calculated band structure. There are at least four possible reasons for the discrepancies; interaction matrix element effects, surface stoichiometry, model shortcomings, and electron-correlation effects. We consider each possibility in rather more detail below.

Interaction matrix element effects would not be expected to produce sufficient changes to account for the major discrepancies, since we do not believe that the As-As first-nearest-neighbor parameters used (see Table II) could be in error by as much as 0.5 eV.

If we next consider the possible influence of surface stoichiometry—i.e., the proportion of As atoms in the outermost layer of an experimentally prepared surface—it is known that a (2×4) RED pattern can be observed over a significant range of stoichiometry.³ However, although we have used different conditions to prepare a (2×4) surface on different occasions, the spectra are all consistent in terms of the energy positions of the peaks, there are only minor variations in intensity. Consequently, this is unlikely to account for the discrepancies between measured and calculated states.

Turning now to the shortcomings of the model,

the obvious problem area is that we have calculated the electronic structure for a (2×1) surface, whereas, of course, we are dealing experimentally with a (2×4) reconstruction. We have pointed out already, however, that the dimerization to produce the $2 \times$ effect is dominant. If we take the (2×1) unit cell, we have initially four broken sp^3 bonds which give rise to the surface states found theoretically. They contain in total $(4 \times \frac{5}{4})$ of an electron (assuming full covalency), so that we have five electrons to place into our four bands (D_i^* , D_{down} , D_{up} , and D_i) resulting from the four broken bonds. Putting two electrons into each of the bands D_i and D_{up} leaves us with only one electron for the dangling-bond band D_{down} resulting from the down-atom dangling lobe. Therefore, this band is only half filled. We have indicated this simple filling of states by the hatchings in the schematic Fig. 12. Again our surface turns out to be metallic. This is, however, no major problem since the experimentally observed (2×4) reconstruction (i.e., the weak $\times 4$ which we have omitted) will fold back all our bands four times, and even the slightest splitting of the bands will make the surface semiconducting. On this basis we would expect the calculation for the (2×1) surface to contain all of the essential features of the surface band structure.

Finally we would note that very recently Duke and Ford²⁸ have applied the Hubbard Hamiltonian to explain discrepancies between calculated and measured surface energy bands of the Si(111)- (1×1) surface. They showed that the discrepancy could be resolved by considering the two-dimensional array of surface dangling bonds as a strongly correlated two-dimensional system. The electron-electron correlation energy was estimated to be 1.1 eV. If we apply the same ideas to the dangling bonds associated with the upper atom of the As dimer (D_{up} ; see Fig. 14) we would, for strong correlation, obtain two parallel bands resulting from D_{up} , with half the dispersion and separated by the electron-electron correlation energy. The center of gravity of the upper split band would remain at the center of gravity of the band D_{up} while the "new" split-off band would be lower in energy by an amount determined from the electron-electron correlation energy. It can be seen from Fig. 10, that a possible way of viewing the experimental results would be to attribute these characteristics to the closely parallel bands between -0.5 and -1.6 eV.

This discussion of correlation effects may also be related to the surface crystallographic model for

the (2×4) reconstruction. If we make the one assumption that the twofold periodicity is introduced solely by an asymmetric As-As dimer formation, the surface atomic arrangement in Fig. 17(b) is the *only* possibility.²⁹ This configuration leads to a lower total energy compared to the (2×1) structure [Fig. 17(a)], and has important implications for correlation effects. Firstly, the distance between second-nearest-neighbor surface atoms (i.e., two "up" atoms) has been increased and although the change is only 2% this would be sufficient to induce a (2×4) reconstruction rather than a (2×1) . However, of itself it would only lead to minor differences in the energy position of the bands. Secondly, the number of second-nearest-neighbor atoms of the same type (i.e., "up" or "down") is reduced by 50% in the (2×4) structure, and this would lead to a significant reduction in the Coulomb correlation energy.

The model we have presented for the electronic and crystallographic structure of GaAs(001)- (2×4) is internally self-consistent with respect to reflection-electron diffraction and photoemission data. It represents only a first attempt and change of detail will inevitably occur. We believe, however, that the basic idea of an asymmetric dimer structure is correct.

ACKNOWLEDGMENTS

We are grateful to P.J. Dobson for permission to discuss his ideas about the surface atomic arrangement of the GaAs(001)- (2×4) structure. We want to thank the technical staff of LURE and of the Laboratoire de l'Accélérateur Linéaire for their help in operating the storage ring. Two of us (A.M. and J.P.) would like to acknowledge finan-

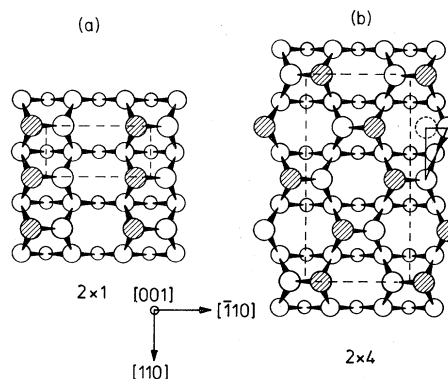


FIG. 17. (2×1) asymmetric dimer structure (a) and the (2×4) full reconstructed asymmetric dimer model (b).

cial support by the Deutsche Forschungsgemeinschaft. One of us (J.F. v.d.V.) is sponsored by the Stichting voor Fundamenteel Onderzoek der Materie with financial support from the Nederlandse

Organisatie voor Zuiver Wetenschappelijk Onderzoek. The measurements were performed at LURE, Université Paris—Sud, 91405 Orsay, France.

- ¹K. Ploog, in *Crystals, Growth, Properties and Applications*, edited by H. C. Freyhardt (Springer, Berlin, 1980), Vol. 3, p. 73.
- ²C. T. Foxon and B. A. Joyce, in *Current Topics in Materials Science*, edited by E. Kaldis (North-Holland, Amsterdam, 1981), p. 1.
- ³J. H. Neave and B. A. Joyce, *J. Cryst. Growth* **44**, 387 (1978).
- ⁴P. Drathen, W. Ranke, and K. Jacobi, *Surf. Sci.* **77**, L162 (1978).
- ⁵J. Massies, P. Etienne, F. Dezaly, and N. T. Linh, *Surf. Sci.* **99**, 121 (1980).
- ⁶R. Z. Bachrach, R. S. Bauer, P. Chiaradia, and G. V. Hansson, *J. Vac. Sci. Technol.* **19**, 335 (1981).
- ⁷J. Massies, P. Devoldere, P. Etienne, and N. T. Linh, *Proceedings of the 7th International Vacuum Congress and Third International Conference on Solid Surfaces*, (IVC, ICSS, Vienna, 1977), p. 639.
- ⁸R. Ludeke, *IBM J. Res. Develop.* **22**, 304 (1978).
- ⁹R. Ludeke and L. Ley, *Physics of Semiconductors—1978*, edited by B. L. H. Wilson (IOP, London, 1979), Vol. 49, p. 1069.
- ¹⁰P. K. Larsen, J. H. Neave, and B. A. Joyce, *J. Phys. C* **12**, L869 (1979).
- ¹¹J. A. Appelbaum, G. A. Baraff, and D. R. Hamann, *Phys. Rev. B* **14**, 1623 (1976).
- ¹²J. Pollmann and S. T. Pantelides, *Phys. Rev. B* **18**, 5524 (1978).
- ¹³I. Ivanov, A. Mazur, and J. Pollman, *Surf. Sci.* **92**, 365 (1980).
- ¹⁴P. K. Larsen, J. H. Neave, and B. A. Joyce, *J. Phys. C* **14**, 167 (1981).
- ¹⁵J. Ihm, M. L. Cohen, and D. J. Chadi, *Phys. Rev. B* **21**, 4592 (1980).
- ¹⁶P. K. Larsen, W. A. M. van Bers, J. M. Bizau, F. Wuilleumier, S. Krummacher, V. Schmidt, and D. Ederer, *Nucl. Instrum. Methods* **195**, 245 (1982).
- ¹⁷J. M. Bizau, Ph.D. thesis, University of Paris—Sud, 1981 (unpublished).
- ¹⁸D. E. Eastman, T.-C. Chiang, P. Heimann, and F. J. Himpsel, *Phys. Rev. Lett.* **45**, 656 (1980).
- ¹⁹J. F. van der Veen, F. J. Himpsel, and D. E. Eastman, *Solid State Commun.* **34**, 33 (1980).
- ²⁰T.-C. Chiang, J. A. Knapp, M. Aono, and D. E. Eastman, *Phys. Rev. B* **21**, 3513 (1980).
- ²¹P. K. Larsen, J. F. van der Veen, A. Mazur, J. Pollmann, and B. H. Verbeek, *Solid State Commun.* **40**, 459 (1981).
- ²²J. Pollmann, *Festkörperprobleme, Advances in Solid State Physics*, edited by J. Treusch (Vieweg, Braunschweig, 1980), Vol. XX, p. 117.
- ²³M. Schmeits, A. Mazur, and J. Pollmann (unpublished).
- ²⁴D. E. Aspnes, C. G. Olson, and D. W. Lynch, *Phys. Rev. B* **12**, 2527 (1975).
- ²⁵D. J. Chadi, *Phys. Rev. Lett.* **43**, 43 (1979); *J. Vac. Sci. Technol.* **16**, 1290 (1979).
- ²⁶S. Froyen and W. A. Harrison, *Phys. Rev. B* **20**, 2420 (1979).
- ²⁷J. R. Chelikowsky and M. L. Cohen, *Phys. Rev. B* **13**, 826 (1976).
- ²⁸C. B. Duke and W. K. Ford, *Surf. Sci.* **111**, L685 (1981).
- ²⁹P. J. Dobson, J. H. Neave, and B. A. Joyce, *Surf. Sci. Lett.* (in press).
- ³⁰D. Y. Chadi, *Phys. Rev. B* **16**, 790 (1977).